Angiogenesis (2016) 19:217–228
DOI 10.1007/s10456-016-9502-0

ORIGINAL PAPER

Oxidative stress induces loss of pericyte coverage and vascular instability in PGC-1α-deficient mice

Nieves García-Quintans[1,3] · Cristina Sánchez-Ramos[1,5] · Ignacio Prieto[1] · Alberto Tierrez[2] · Elvira Arza[2] · Arantzazu Alfranca[2,4] · Juan Miguel Redondo[2] · María Monsalve[1]

Received: 23 September 2015 / Accepted: 19 February 2016 / Published online: 7 March 2016

Abstract Peroxisome proliferator-activated receptor γ coactivator 1α (PGC-1α) is a regulator of mitochondrial oxidative metabolism and reactive oxygen species (ROS) homeostasis that is known to be inactivated in diabetic subjects. This study aimed to investigate the contribution of PGC-1α inactivation to the development of oxygen-induced retinopathy. We analyzed retinal vascular development in PGC-1α$^{-/-}$ mice. Retinal vasculature of PGC-1α$^{-/-}$ mice showed reduced pericyte coverage, a de-structured vascular plexus, and low perfusion. Exposure of PGC-1α$^{-/-}$ mice to hyperoxia during retinal vascular development exacerbated these vascular abnormalities, with extensive retinal hemorrhaging and highly unstructured areas as compared with wild-type mice. Structural analysis demonstrated a reduction in membrane-bound VE-cadherin, which was suggestive of defective intercellular junctions. Interestingly, PGC-1α$^{-/-}$ retinas showed a constitutive activation of the VEGF-A signaling pathway. This phenotype could be partially reversed by antioxidant administration, indicating that elevated production of ROS in the absence of PGC-1α could be a relevant factor in the alteration of the VEGF-A signaling pathway. Collectively, our findings suggest that PGC-1α control of ROS homeostasis plays an important role in the regulation of *de novo* angiogenesis and is required for vascular stability.

Keywords PGC-1α · Retinopathy · Vascular stability · Angiogenesis · ROS

Abbreviations

AKT	Protein kinase B
cdh-5	Cadherin 5
DAPI	4′,6-diamino-2-fenilindol
dll1	Delta-like-1
dll4	Delta-like-4
EUK-189	Eukarion-189
hes1	Hairy and enhancer of split-1
hey1	Hairy/enhancer of split related with YRPW motif protein 1
HNE	4-Hydroxynonenal
HIF-1α	Hypoxia inducible factor-1α
IF	Immunofluorescence
IsoB4	Isolectin B4
NG2	Neuron-glial antigen 2
NICD	NOTCH intracellular domain
P	Phosphorylated
PGC-1α	Peroxisome proliferator-activated receptor γ-coactivator 1α
(P17)	Postnatal day 17
ROS	Reactive oxygen species

Electronic supplementary material The online version of this article (doi:10.1007/s10456-016-9502-0) contains supplementary material, which is available to authorized users.

✉ María Monsalve
mpmonsalve@iib.uam.es

[1] Instituto de Investigaciones Biomédicas "Alberto Sols" (CSIC-UAM), Arturo Duperier 4, Room 1.3.2, 28029- Madrid, Spain

[2] Fundación Centro Nacional de Investigaciones Cardiovasculares Carlos III, Melchor Fernández Almagro 3, 28029- Madrid, Spain

[3] Present Address: Centro de Biología Molecular Severo Ochoa (CSIC-UAM), Nicolas Cabrera 1, 28049- Madrid, Spain

[4] Present Address: Fundación para la Investigación Biomédida del Hospital Universitario La Princesa, Diego de León 62, 28006- Madrid, Spain

[5] Present Address: Fundación Centro Nacional de Investigaciones Cardiovasculares Carlos III, Melchor Fernández Almagro 3, 28029- Madrid, Spain

Smooth muscle actin	SMA
VEGF-A	Vascular endothelial growth factor-A
VE-Cadherin	Vascular endothelial cadherin
flk1 (gene), VEGFR2 (protein)	Vascular endothelial growth factor receptor 2

Introduction

The importance of protecting the body from the most common metabolic disorders including obesity and type 1 and type 2 diabetes cannot be overstated, and their prevalence continues to increase yearly and worldwide. Dysfunctions of the human vascular tree are the major sources of morbidity and mortality. Generally, the damaging effects can be separated into macrovascular (coronary artery disease, peripheral arterial disease, and stroke) and microvascular (nephropathy, neuropathy, and retinopathy) injury [1]. Diabetic retinopathy is one of the most common microvascular complications of diabetes and is a leading cause of $\sim$10,000 new cases of blindness every year in the USA alone [2].

Metabolic disorders are characterized fundamentally by a poor use of mitochondria as a source of ATP and a preponderance of anaerobic glycolysis [3, 4]. This decrease in mitochondrial function is mediated principally by the down-regulation and functional inactivation of the transcriptional coactivator peroxisome proliferator-activated receptor gamma coactivator-1-α (PGC-1α) [5, 6], a master regulator of genes involved in oxidative metabolism. Loss of PGC-1α activity results in an increase in mitochondrial-derived reactive oxygen species (ROS) [7], and elevated ROS levels (oxidative stress) have been found in the majority of vascular complications associated with metabolic disorders.

Our previous results showed that PGC-1α was present in vascular endothelial cells (ECs), and its levels were reduced by hyperglycemia. Furthermore, PGC-1α could coordinate EC oxidative metabolism and antioxidant capacity [8], suggesting that PGC-1α could play a key role in the physiology of the vascular endothelium. Additional studies from our laboratory showed that, at least in vitro, PGC-1α was a negative regulator of EC migration indicating that PGC-1α activity could be important for the control of vascular stability and angiogenesis. Accordingly, activation of PI3K-AKT signaling in response to angiogenesis mediators resulted in the down-regulation of PGC-1α, leading to increased mitochondrial ROS levels and enhanced EC migration [9]. ROS are acknowledged as important signaling mediators regulating cell proliferation and migration [10].

In this study we aimed to characterize the role of PGC-1α as a regulator of mitochondrial function and ROS in the control of angiogenesis and to evaluate its possible contribution to vascular diseases, particularly diabetic retinopathy.

We found that the retinal vasculature in PGC-1$\alpha^{-/-}$ animals exhibited characteristics of an unstable phenotype that was exacerbated upon exposure to an oxygen-induced retinopathy (OIR) protocol. Crucially, this phenotype could be partially rescued by antioxidant treatment, suggesting that excessive ROS production likely plays a role in microvascular instability.

Materials and methods

Animal handling

C57BL/6 PGC-1$\alpha^{+/+}$ and PGC-1$\alpha^{-/-}$ were used. All animal experiments were performed in accordance with the ARVO Statement for the Use of Animals in Ophthalmic and Vision Research. Animal protocols were approved by the Institutional Animal Care and Use Committee of the CNIC and the CSIC. All procedures conformed to the Declaration of Helsinki and the NIH guidelines for animal care and use (NIH publication No. 85–23).

Oxygen-induced retinopathy (OIR)

Ischemic retinopathy was generated according to an established OIR protocol [11]. In brief, p7 pups were transferred with their mothers to a hyperoxia chamber set at 70 % O_2 where they stayed for 5 days and then returned to normoxic conditions. P17 pups were killed. EUK-189 (30 mg/kg in PBS) was administered daily by intraperitoneal injection from day 4 to day 7 and from day 12 to day 17. EUK-189 is a salen–manganese complex and superoxide dismutase/catalase mimetic that has been shown to be effective as antioxidant in vivo and in the inactivation of mitochondrial ROS [12].

Retina isolation

Postnatal day 17 (P17) pups were euthanized in a CO_2 chamber. Eyes were enucleated and fixed in 4 % paraformaldehyde (PFA) in PBS at 4 °C for 48 h.

Whole-mount staining

Retinas were postfixed for 1 h in fixative solution, blocked, and permeabilized in PBS containing 1 % bovine serum albumin (BSA) and 0.5 % Triton X-100, for 2.5 h at RT. The staining solution was PBS pH 6.8 with 0.1 mM $CaCl_2$, 0.1 mM $MgCl_2$ and 0.1 mM $MnCl_2$ and the antibodies

used were: FITC-conjugated anti-*Griffonia simplicifolia* Isolectin B_4 from Sigma-Aldrich (L2895), anti-NG2 from Millipore (#AB5320), and Cy3-conjugated anti-smooth muscle α-actin from Sigma-Aldrich (C6198). Staining was performed for 48 h at 4 °C. For VE-cadherin staining (#550548, anti-CD144, BD PharMingen), the retinas were first blocked and permeabilized with PBS containing 5 % FBS and 0.3 % Triton X-100 and then washed for 1.5 h in PBS. Incubations with fluorescent-tagged secondary antibodies were performed for 2 h at RT and included Alexa-fluor 647 chicken anti-rabbit (Invitrogen) and Alexa-fluor 488 chicken anti-rat (Invitrogen). DAPI (1:1000) (Invitrogen) was used for nuclear visualization. Retinal images were acquired with a Zeiss LSM 700 or LSM 710. Unless otherwise indicated, images shown are maximal projections of z-stacks covering the whole retinal section.

Eye cross sections

Eyes were enucleated, fixed (70 % ethanol, 10 % formalin and 5 % acetic acid) for 48 h, and embedded in paraffin. Sections of 4 μm were stained with hematoxylin and eosin (H&E). Images were acquired with a Nikon 90i microscope.

Vascular perfusion and leakage

Mice were injected via tail vein or retro-orbitally with 100 μl FITC–dextran (FD2000S; Sigma-Aldrich) at a concentration of 40 mg/ml in PBS. The animals were killed 5 min later. Images of retinal flat mounts were obtained by confocal microscopy. Retinal segments were merged to generate a whole retinal image using Nikon A1R software.

Matrigel angiogenesis assay

Matrigel and growth factor-reduced (GFR) Matrigel (10 mg/ml) were mixed with 25 U/ml heparin (Sigma-Aldrich). VEGF-A (8 μg/ml) was added to GFR Matrigel as indicated. Three hundred microliters of the mixture was injected subcutaneously. Implants were harvested after 2 weeks and fixed in formalin for 12 h. Half of the sample was embedded in OCT and frozen. The other half was embedded in paraffin. Samples were analyzed by immunofluorescence using the previously indicated antibodies and an anti-CD31 antibody to assess blood vessel formation and vascular patterns (#557355, BD PharMingen).

Cell culture

Mouse lung endothelial cells (MLECs) were obtained and cultured as described [9]. Wild-type and PGC-$1^{-/-}$ MLEC were cultured in round glass coverslips, fixed with PFA 4 %, permeabilized, and blocked with 10 % FBS, 0.3 % Triton X-100 in PBS and were incubated with an antibody against Tomm22 (HPA003037, Sigma-Aldrich). Cells were counterstained with DAPI (Molecular Probes) and mounted with ProLong (Molecular Probes). Photographs were taken with a spectral confocal microscope LSM710 (Zeiss) and analyzed using ImageJ software. Whole-cell extracts were analyzed by western blotting using antibodies directed against PGC-1α (#ST1202, Millipore) and 4-hydroxynonenal (HNE) (#HNE11, Alpha Diagnostic Int.).

Protein extraction and western blotting was performed as previously described [13]. Specific antibodies used were: HIF-1α (#610958, BD Transduction Laboratories), VEGF-A, (VG-1, Santa Cruz), VEGF-R2 (#55B11, 1:1000), P-VEGFR2 (# 2471, 1:1000), NICD (#4147, 1:1000), AKT (#2920), and phosphorylated AKT-Ser^{473} (#4060) (1:2000), all from Cell Signaling Technology, and *β*-actin (A 5441, Sigma).

RNA isolation and qRT-PCR were performed as previously described [13].

Specific oligonucleotides were:

vegf-a
Forward: 5′-GAAGTCCCATGAAGTGATCAAGT-3′
Reverse: 5′-CTTTGGTCTGCATTCACATCT-3′
flk1
Forward: 5′-CTCTCCACCTTCAAAGTCTCAT-3′
Reverse: 5′-GGCTTTGTGTGAACTCGGACAA-3′
dll 4
Forward: 5′-ACCAACTCCTTCGTCGTCAG-3′
Reverse: 5′-AGGGTGTCATTTTGCTCGTCT-3′
notch 1
Forward: 5′-GGTGTCTTCCAGATCCTGCT-3′
Reverse: 5′-AGTCTCCTCCTTGTTGTTCTG-3′
dll 1
Forward: 5′-CAATGGAGGACGATGTTCAG-3′
Reverse: 5′-CAGGTAAGAGTTGCCGAGGT-3′
hes 1
Forward: 5′-CTGCTACCCCAGCCAGTGT-3′
Reverse: 5′-CGGAGGTGCTTCACAGTCATT-3′
hey 1
Forward: 5′-GAAAAGACGGAGAGGCATCAT-3′
Reverse: 5′-GTGCGCGTCAAAATAACCTT-3′
jagged 1
Forward: 5′-CAGTGCCTCTGTGAGACCAA-3′
Reverse: 5′-GTTATGGCAGGGGTCAGAGA-3′
cdh 5 (VE-cadherin)
Forward: 5′-CCAAATCGTGAAAGGAAATGA-3′
Reverse: 5′-CAGGCACCGAAAATGTGTATG-3′

Image analysis

ImageJ software was used to analyze western blots signals and for global determination of areas in immunofluorescent

images, vascular shape analysis of Matrigel plugs, and membrane/cytosol ratios of VE-cadherin. AngioTool was used for analysis of retinal vascular plexus. H&E images were reviewed manually.

Statistics

Data are expressed as mean ± SD. Statistical significance was evaluated by analysis of variance or a nonparametric test, as appropriate. Values were considered statistically significant at $p < 0.05$; $n = 3$ independent experiments, where $n = 3$–5 animals per group in each independent experiment.

Results

To assess the functional consequences of PGC-1α deficiency, we analyzed the retinal vasculature of PGC-1$\alpha^{-/-}$ pups. The retinal vasculature develops postnatally in the mouse and at P17 angiogenesis initiating at the center of the retina is expected to have reached the retinal edge. No gross structural differences could be detected in the vascular network of retinas from P17 PGC-1$\alpha^{-/-}$ mice compared with wild-type littermates as visualized by FITC-isolectin B4 immunohistochemistry, indicating a lack of major developmental problems (Fig. 1a, top panel). Furthermore, no reduction in the density of the vascular plexus was detected (Fig. 1a, top panel). We analyzed pericyte coverage in the retina by immunohistochemistry using an anti-NG2 antibody that labels pericytes in the micro- and macrovasculature and an anti-SMA antibody that labels smooth muscle cells of large blood vessels. No differences were detected in SMA staining between retinas from PGC-1$\alpha^{-/-}$ and PGC-1$\alpha^{+/+}$ mice (Fig. 1a, top panel). However, pericyte coverage was markedly reduced in PGC-1$\alpha^{-/-}$ retinas stained with NG2, and this reduction was more dramatic in the center of the retina than on the retinal edge where active angiogenesis was still ongoing (Fig. 1a, top panel). This interesting finding suggested that pericytes were initially recruited during the angiogenesis process and then lost. To discern the functional consequences of reduced pericyte coverage, we examined the microvascular structure. Retinas of PGC-1$\alpha^{-/-}$ mice had substantial disorganization of the microvasculature, with many ghost-like blood vessels unlikely to be perfused (Fig. 1a, mid-panel). Consistently, average lacunarity in the primary plexus, but not in the inner plexus, was significantly reduced in PGC-1$\alpha^{-/-}$ retinas. Moreover, junction density was increased whereas average vessel length was not significantly altered (Fig. 1a, mid-panel, and Online Supp. Figure 1).

As the in vitro characterization of PGC-1$\alpha^{-/-}$ ECs suggested a greater propensity to form tip cells, we examined retinal tip cell formation in PGC-1$\alpha^{-/-}$ retinas. As expected, tip cells were found only in the retinal edge in wild-type mice indicating active angiogenesis, with filopodia decorating only the tips of elongated cells (Fig. 1a, bottom panel). In contrast, PGC-1$\alpha^{-/-}$ retinas contained tip cells in the middle regions of the retina and on phalanx cells in the middle of a vessel, and with large numbers of filopodia close to the cell body (Fig. 1a, bottom panel). This phenotype, which is characteristic of excessive tip activity, is typically associated with dense vascular plexus and within this context, could be related to the low stability of the blood vessels.

Because poor formation of intercellular junctions can result in an unstable microvasculature, we examined endothelial intercellular junction interactions by immunostaining for VE-cadherin. Nevertheless, VE-cadherin staining showed that its normal membrane distribution was preserved in PGC-1$\alpha^{-/-}$ animals (Fig. 1b, top panel).

Examination of retinal cross sections stained with H&E revealed a normal retinal structure in PGC-1$\alpha^{-/-}$ mice, although a slight disorganization of the ganglion cell layer could be observed with loss of epithelial-like structure that could be related to poor visual function (Fig. 1b, bottom panel). The origin of these differences was not investigated further.

To determine the impact of the reduced vascular stability on general vascular perfusion, we analyzed retinal perfusion using retro-orbitally injected FITC–dextran. As expected, a marked and general reduction in the perfusion in PGC-1$\alpha^{-/-}$ mice was detected, with a significant reduction in both the mean fluorescence intensity and the detectable area covered by vascular structures (Fig. 1c).

To determine whether the low vascular stability of PGC-1$\alpha^{-/-}$ retinas might be due to an alteration in VEGF-A levels or activity of its downstream effectors, we monitored the expression of VEGF-A together with the activity/phosphorylation of its main angiogenesis receptor, VEGFR2, and its main effectors, AKT and NICD. Levels of VEGF-A in PGC-1$\alpha^{-/-}$ retinas were comparable with retinas from control animals. In contrast, increased levels of total and phosphorylated VEGFR2, phosphorylated AKT, and the active form of NOTCH1, NICD, were detected (Fig. 1d). This result was unexpected, since PGC-1α is known to induce the expression of VEGF-A [14]. We therefore measured *vegf-a* mRNA levels. Consistent with previous reports [15, 16], we detected lower levels in PGC-1$\alpha^{-/-}$ mice (Online Supp. Figure 2). We also analyzed *flk1* (VEGFR2) and *cdh5* (VE-cadherin) mRNA levels. Although *cdh5* levels were on average somewhat lower in PGC-1$\alpha^{-/-}$ mice, no significant differences were detected relative to wild-type mice. These findings suggested that posttranscriptional regulation could be responsible for the observed differences in protein levels and were consistent

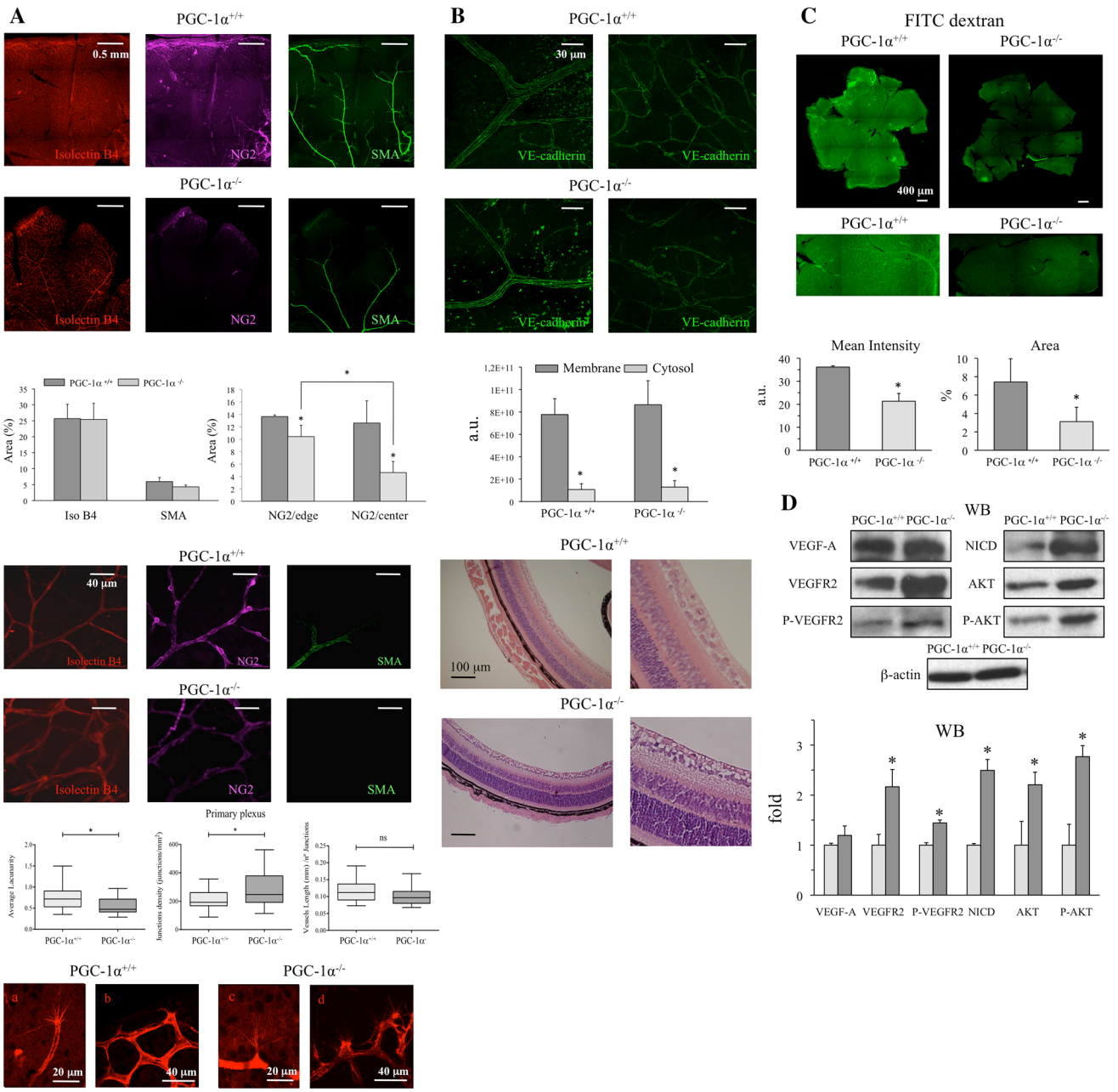

Fig. 1 Reduced pericyte coverage, structural disorganization, and impaired perfusion in retinas from PGC-1α$^{-/-}$ mice despite normal VEGF-A levels. **a** Flat-mount retinas from wild-type and PGC-1α$^{-/-}$ mice were immunostained with Isolectin B4 (ECs), NG2 (pericytes), SMA (smooth muscle), and VE-cadherin (EC tight junctions). **a** *top* Center to edge sections show general vascular system (×10 objective). **a** *Mid* Arterioles and microvasculature (×40 objective). **a** *bottom* Tip cells (×60 objective). **b** *Top* VE-cadherin staining in the microvasculature (×40 objective). **b** *Bottom* H&E staining of retina cross sections from wild-type and PGC-1α$^{-/-}$ mice. **c** Flat-mount retinas from wild-type and PGC-1α$^{-/-}$ mice perfused with FITC dextran; the lower panel shows higher magnification images. **d** Western blot analysis of retinal extracts of relevant proteins in the control of angiogenesis: VEGF-A, VEGFR2, NICD, and AKT. Data are from three independent experiments, $n = 3$–5 animals per group in each independent experiment. Data are mean ± SD. *$p \leq 0.05$ versus control

with an enhanced constitutive activity of VEGFR2 (Fig. 1g, Online Supp. Figure 2).

It was possible that these findings could result from increased levels of NOTCH1 ligands or elevated *Notch1* expression. This second scenario, however, was unlikely since the expression levels of *notch1* and its ligands *jagg1, dll1*, *and dll4* were not increased in PGC-1α$^{-/-}$ retinas; indeed, *dll4* expression was decreased. Furthermore, the elevated level of NICD was not associated with an increased expression of the NICD target genes *hes1* and

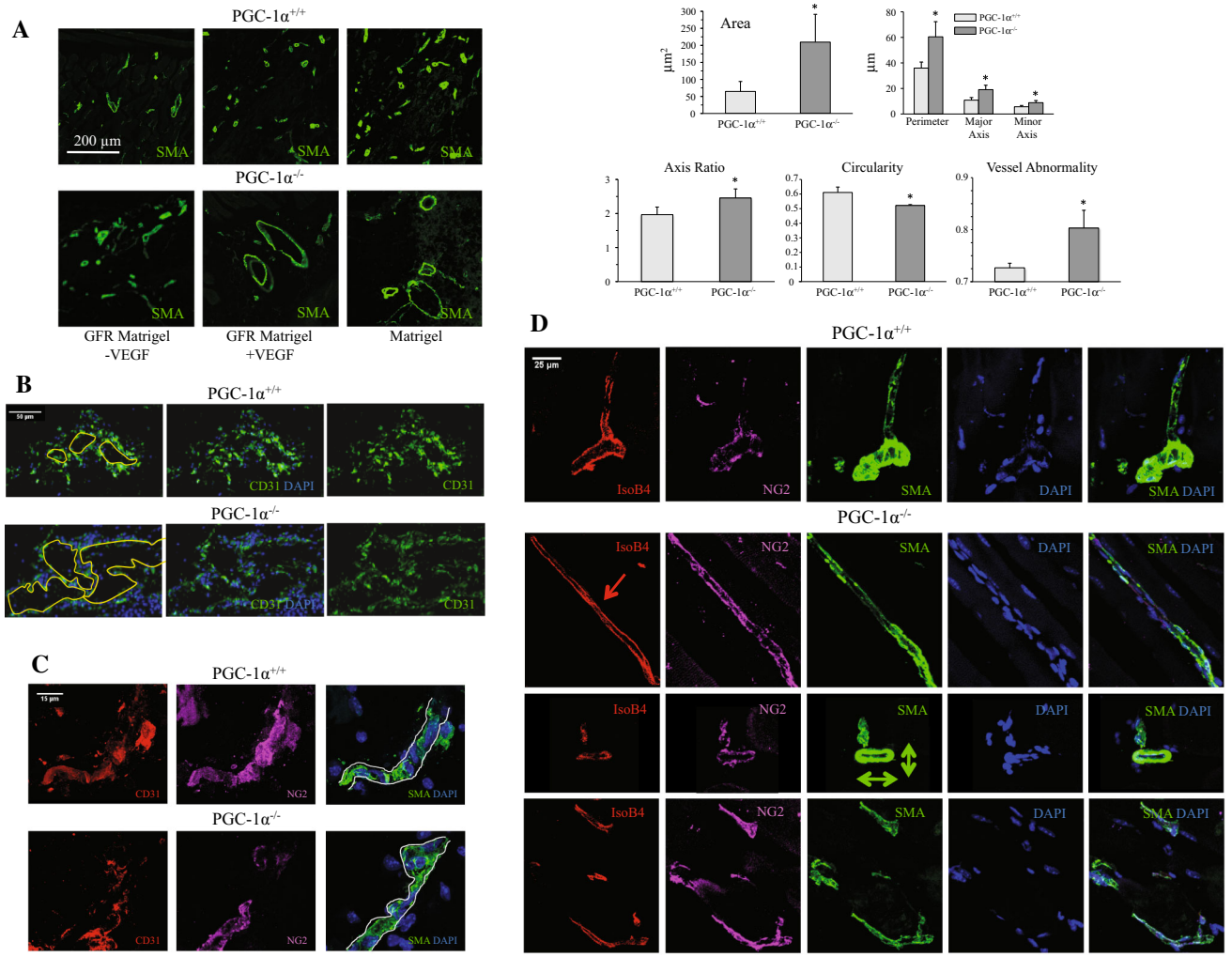

Fig. 2 Absence of PGC-1α results in the formation of enlarged and irregular blood vessels in Matrigel implants. **a–d** Immunofluorescence stain of Matrigel implants from wild-type and PGC-1α$^{-/-}$ mice. **a** SMA stain of Matrigel implants and GFR Matrigel implants with or without VEGF-A (×25 objective). **b** CD31 and DAPI (×40 objective **c** CD31, NG2, DAPI (×60 objective). **d** IsoB4, NG2, SMA, DAPI (×40 objective). Data are from three independent experiments, *n*= 3–5 animals per group in each independent experiment. Data are mean ± SD. *$p \leq 0.05$ versus control

hey1, which were comparable between wild-type and PGC-1α$^{-/-}$ mice, possibly suggesting a reduced transcriptional activity of NICD in PGC-1α$^{-/-}$ mice (Fig. 1g, Online Supp. Figure 2). Taken together, these observations suggested that the reduced vascular density observed in PGC-1α$^{-/-}$ mice did not result from changes in VEGF-A or NICD.

To evaluate the role of PGC-1α in the control of angiogenesis in vivo, in a system where VEGF-A could be provided in a controlled manner, we used a Matrigel plug assay of neovessel formation and injected this matrix subcutaneously into wild-type and PGC-1α$^{-/-}$ mice. Three conditions were tested: Matrigel rich in growth factors, including VEGF, and GFR Matrigel with or without added VEGF. Angiogenesis was allowed to proceed for 2 weeks and plugs were extracted and analyzed to evaluate the number, size, and shape of neovessels. No differences were detected in the number of neovessels between wild-type and PGC-1α$^{-/-}$ mice (SMA staining; data not shown). In contrast, significantly larger blood vessels were detected in PGC-1α$^{-/-}$ mice under all conditions tested (Fig. 2a and Online Supp. Figure 3). Furthermore, the shape of the vessels was more irregular in PGC-1α$^{-/-}$ animals, with larger differences in the axis ratio, and reduced circularity and larger vessel abnormality values (Fig. 2a). The nature of the vessels was confirmed by staining with the endothelial markers CD31 and IsoB4 (Fig. 2b–d). Pericyte coverage, determined by NG2 staining, was also more irregular in PGC-1α$^{-/-}$ mice (Fig. 2c). Figure 2d contrasts a typical branching wild-type vessel on the top panel, with

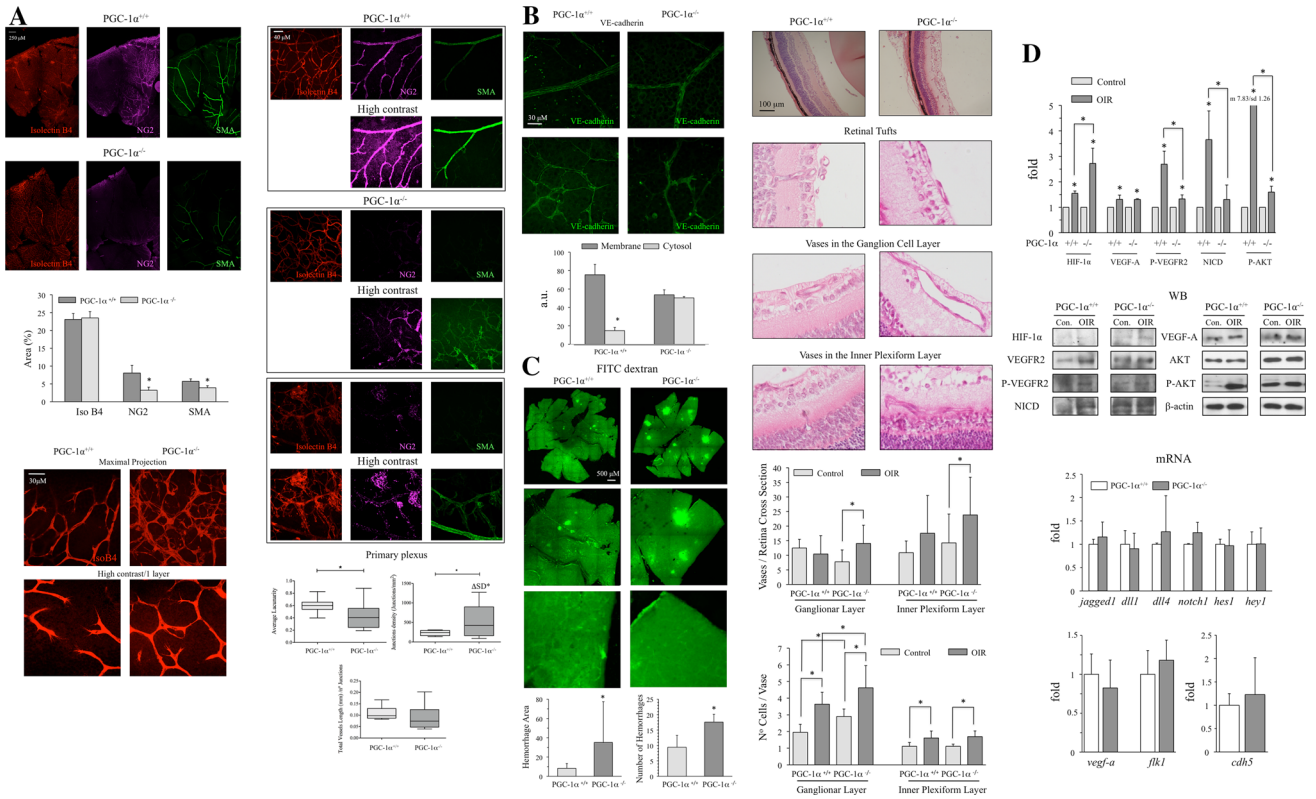

Fig. 3 OIR in PGC-1α$^{-/-}$ mice severely disrupts the retinal vascular structure, but does not induce VEGF-A levels or activity. Abnormally large blood vessels in the ganglionar layer, loss of endothelial junctions, highly irregular vascular plexus with poor pericyte coverage, and large hemorrhagic areas are observed in PGC-1α$^{-/-}$ mice. **a** Flat-mount retinas from wild-type and PGC-1α$^{-/-}$ mice where immunostained with Isolectin B4, NG2, SMA, and VE-cadherin. **a** *top* Center to edge sections show general vascular system (×10 objective). **a** *Mid* Arterioles and microvasculature (×40 objective). **a** *Bottom* Tip cells (×60 objective). **b** *Left* VE-cadherin stain in the microvasculature (×40 objective). **b** *right* H&E stain of retina cross sections from wild-type and PGC-1α$^{-/-}$ mice. **c** Flat-mount retinas from wild-type and PGC-1α$^{-/-}$ mice perfused with FITC dextran; lower panels show higher magnification images. **d** *Top* Western blot analysis of retinal extracts of relevant proteins in the control of angiogenesis: VEGF-A, VEGFR2, NICD, and AKT. **d** *bottom* qRT-PCR analysis of mRNA levels of relevant genes in the control of angiogenesis. Data are from three independent experiments, n= 3–5 animals per group in each independent experiment. Data are mean ± SD. *$p \leq 0.05$ versus control

examples of the anomalies that we could find in PGC-1α$^{-/-}$ mice, from top to bottom we can see, the irregularity of the lumen in a lengthwise section of a vessel, with a constriction point, a cross section of a collapsed vessel, and a dilated irregular vessel in cross section.

To further evaluate the role played by PGC-1α in the control of vascular stability and the response to VEGF-A, we used the oxygen-induced retinopathy model (OIR) where one-week-old mice and their mothers are first exposed to hyperoxia (70 % O_2) for 5 days and then returned to normoxic conditions for a further 5 days. This generates a hypoxia inducible factor-1α (HIF-1α)-dependent overproduction of VEGF-A in the developing retinal vasculature, which promotes neovascularization in the retinal periphery. As such, this model recapitulates the vascular anomalies found in proliferative diabetic retinopathy [17].

Flat-mount retinas from 17-day-old OIR wild-type and PGC-1α$^{-/-}$ mice were immunostained with isolectin B4, NG2, and SMA antibodies and examined by confocal microscopy. OIR decreased the general vascular density both in wild-type and PGC-1α$^{-/-}$ mice (Fig. 3a, top panel, Online Supp. Figure 4). OIR resulted in the loss of pericyte coverage and this reduction was more dramatic in PGC-1α$^{-/-}$ retinas (Fig. 3a). SMA staining was also more reduced by OIR in PGC-1α$^{-/-}$ than in wild-type retinas, suggesting that vascular instability induced by the loss of PGC-1α extended also to the macrovasculature (Fig. 3a, top panel). Closer examination of isolectin B4-stained vascular structures revealed that, compared with wild-type, PGC-1α$^{-/-}$ retinas contained highly-disorganized areas (Fig. 3a, mid-panel). High-contrast imaging indicated that pericyte coverage in OIR wild-type animals was low but structurally organized (Fig. 3a, mid-panel). In contrast,

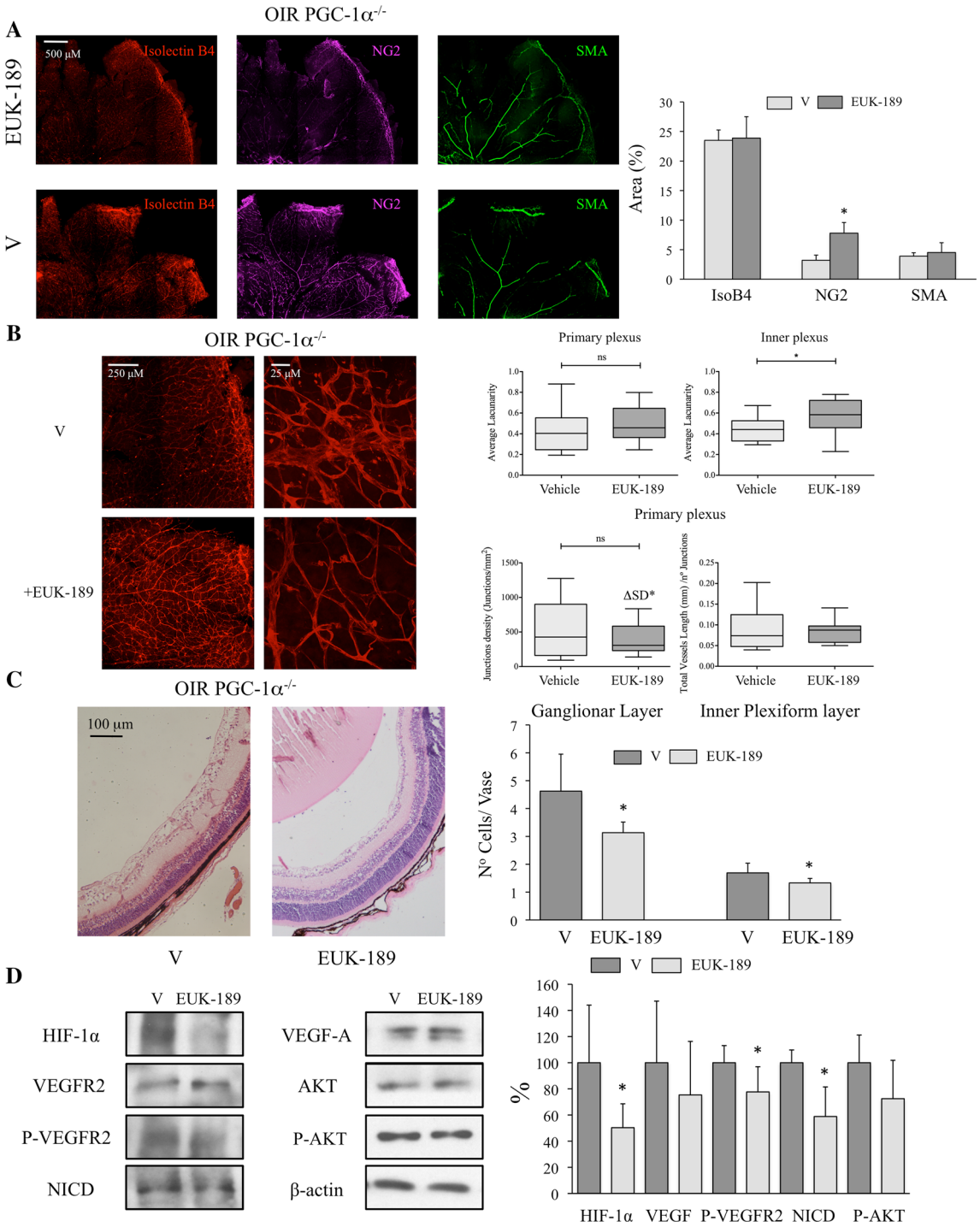

Fig. 4 Severity of OIR in PGC-1α$^{-/-}$ mice is prevented by EUK-189 treatment. **a–c** Flat-mount retinas from wild-type and PGC-1α$^{-/-}$ mice were immunostained with Isolectin B4 (endothelial cells), NG2 (pericytes), SMA (smooth muscle cells), and VE-cadherin (tight junctions of ECs). **a** Center to edge sections of the vascular system (×10 objective). **b** Arterioles and microvasculature (×40 objective). **c** H&E stain of retina cross sections from wild-type and PGC-1α$^{-/-}$ mice. **d** Western blot analysis of retinal extracts of relevant proteins in the control of angiogenesis. Data are from three independent experiments, n= 3–5 animals per group in each independent experiment. Data are mean ± SD. *$p \leq 0.05$ versus control. *ns* not significant

OIR PGC-1α$^{-/-}$ mice exhibited an aberrant distribution of pericytes with large neovascular structures showing NG2 and SMA staining. Quantitative analysis showed reduced lacunarity in the primary plexus and increased junction density, in the absence of significant changes in the average vessel length, in OIR PGC-1α$^{-/-}$ retinas, (Fig. 3a, mid-

panel). Additionally, a significant increase in the standard deviation (SD) of the junction density was detected in OIR PGC-1$\alpha^{-/-}$ mice, indicating a more marked disorganization of the retinal plexus. Analysis of z-stack layers of high-resolution images allowed the identification of tip cells. In wild-type retinas tip cells were typically found in pairs, with filopodia pointing toward each other, and with both cells located in the same vascular plexus, whereas tip cells showed no apparent directionality in PGC-1$\alpha^{-/-}$ retinas (Fig. 3a, bottom panel).

Endothelial intercellular junctions were evaluated by VE-cadherin staining. In wild-type retinas normal, membrane-bound, staining was preserved, while PGC-1$\alpha^{-/-}$ mice exhibited diffuse (cytosolic) VE-cadherin staining in both capillaries and larger blood vessels (Fig. 5b, left panel, Online Supp. Figure 5). This finding suggested a predominantly intracellular location of VE-cadherin in PGC-1$\alpha^{-/-}$ mice, with massive loss of intercellular junctions and vascular instability.

As previously reported, OIR in wild-type mice induces the formation of penetrating capillaries across the plexiform layer and ECs tufts on the inner limiting membrane of the retina extending into the vitreous, which together contribute to the neovascularization process [11]. Using H&E staining to survey the vascular architecture after OIR, anomalous blood vessel formation was also detected in PGC-1$\alpha^{-/-}$ mice (Fig. 3b, right panel). Indeed, no substantial differences were found between wild-type and knockout mice in the number of tufts (Online Supp. Figure 6). However, notable differences were found in the ganglionar and inner plexiform layers. PGC-1$\alpha^{-/-}$ mice responded to the OIR protocol with a more dramatic increase in the number of anomalous blood vessels than wild-type mice (Fig. 3b, right panel). Moreover, the vessels in the ganglionar layer were larger in PGC-1$\alpha^{-/-}$ mice (Fig. 3b, right panel), and, on occasion, hemorrhagic (Online Supp. Figure 7). All these observations are consistent with the results shown in Fig. 2 indicating that the loss of PGC-1α has a particular high impact on the structure of the newly formed vessels, rather than on the vessel number.

To evaluate the functional relevance of these findings, we analyzed vascular perfusion and permeability by tail vein injection of FITC–dextran. A reduced vascular perfusion together with the appearance of hemorrhagic lesions was observed in wild-type mice (Fig. 3c), as previously described for OIR. PGC-1$\alpha^{-/-}$ mice exhibited a more severe phenotype with extended non-perfused areas together with a greater number of larger hemorrhages (Fig. 3c). The three images of Fig. 3c show from top to bottom the whole retina, where we can appreciate the elevated number of hemorrhages in PGC-1$\alpha^{-/-}$ mice, a higher amplification image, focused on the size comparison between hemorrhagic lesion in wild-type and PGC-1$\alpha^{-/-}$ mice and a further zoom in image to visualize the absence of perfused vessels in extensive areas of PGC-1$\alpha^{-/-}$ mouse retinas. The graph at the bottom shows the quantification of the number and the size of the hemorrhages.

To investigate whether these anomalies might be related to alterations in the induction of angiogenesis mediators, we measured HIF-1α, VEGF-A, and its downstream effectors in retinas. As expected, OIR increased the levels of HIF-1α and VEGF-A protein, increased the phosphorylation of VEGFR2 and AKT, and also increased the levels of NICD in wild-type mice (Fig. 3d, top panel). In PGC-1$\alpha^{-/-}$ mice, OIR resulted in a more marked induction of HIF-1α and a significantly attenuated increase in phosphorylated VEGFR2, phosphorylated AKT and NICD (Fig. 3d, top panel), while VEGF-A was induced to the same extent in wild-type and PGC-1$\alpha^{-/-}$ retinas. These results suggested that HIF-α induction is boosted in PGC-1$\alpha^{-/-}$ mice, possibly indicating that PGC-1α is working as a negative regulator of HIF-α protein levels. In fact, HIF-1α is positively regulated by ROS and ROS are elevated in the absence of PGC-1α. They also indicate that HIF-1α can induce VEGF-A levels both in the presence and in the absence of PGC-1α. However, while the wild-type mice respond to elevated levels of VEGF-A induced by OIR with an corresponding activation of the VEGFR2 and its downstream effectors, this activation is significantly blunted in PGC-1α mice, suggesting a poorer response to VEGF-A. Retinal mRNA expression levels of the NOTCH1 ligands *jagged1*, *dll4*, and *dll1*, of *notch1* itself, its target genes *hes1* and *hey1, vegf-a, flk1*, and *cdh5* were also evaluated. No significant differences were found between wild-type and PGC-1$\alpha^{-/-}$ mice, suggesting that the phenotype observed was not likely to be attributable to differences in NOTCH1 activity (Fig. 3d, bottom panel). Collectively, these results suggest that PGC-1α-deficient mice are more sensitive to OIR, likely due to an inability to form stable/mature blood vessels.

PGC-1$\alpha^{-/-}$ MLECs migrate faster than wild-type cells due to an overproduction of ROS [9]. Indeed, ROS are important players in EC migration and proliferation [18, 19]. Thus, we evaluated whether the vascular instability in PGC-1$\alpha^{-/-}$ mice could be attributed to an excess of ROS. To test this idea, the antioxidant EUK-189 was administered to OIR PGC-1$\alpha^{-/-}$ mice daily by intraperitoneal injection from day 4 to day 7, when the pups entered the hyperoxia chamber, and from day 12 to day 17 when they were returned to normoxia. Flat-mount retinas from 17-day-old OIR-treated PGC-1$\alpha^{-/-}$ mice were immunostained with isolectin B4, NG2, and SMA antibodies. Endothelial staining with isolectin showed that EUK-189 did not alter the vascular density of OIR-treated PGC-1$\alpha^{-/-}$ mice but improved the structural organization of the

vascular plexus (Fig. 4a). NG2 staining indicated an improvement in coverage in EUK-189-treated mice (Fig. 4a). SMA staining was marginally enhanced by EUK-189, although differences were not significant (Fig. 4a). Structural analysis revealed that EUK-189 treatment increased the average lacunarity in the inner plexus and decreased the junction density, as well as its variability, in the primary plexus without significantly changing the total vessel length (Fig. 4b). Nevertheless, EUK-189 failed to fully restore the microvascular structure in OIR-treated PGC-1$\alpha^{-/-}$ mice, and a significant number of abnormally twisted capillaries were apparent (Fig. 4b). The number of tip cells was reduced in EUK-189-treated mice, and the tip cells showed a reduced number of filopodia but did not show the polarity normally found in tip cells where filopodia can be found only on one side of the cell, while the other is firmly associated with a stalk cell (Online Supp. Figure 8). The effect of EUK-189 on the vascular anomalies induced by OIR was further analyzed by H&E staining of retinal cross sections. The size of the abnormal blood vessels in the ganglion cell layer and the inner plexiform layer was reduced by EUK-189 treatment (Fig. 4c). These observations suggested that the reduced vascular stability provoked by the absence of PGC-1α was partially restored by antioxidant treatment.

Finally, to test whether this structural recovery was associated with a restoration of a normal VEGF-A-dependent response, we measured protein (Fig. 4d) and mRNA levels (Online Supp. Figure 9) of VEGF-responsive factors. EUK-189 treatment significantly reduced the levels of HIF-1α, phosphorylated VEGFR2, and NICD, but had no effect on VEGF-A protein levels, suggesting that in vivo treatment with EUK-189 improved VEGF-A signaling in PGC-1$\alpha^{-/-}$ mice. EUK-189 treatment did not produce significant changes in the mRNA levels of *notch1*, its ligands *dll1*, *dll4*, its targets *hes1*, *hey1*, or *flk1* and *cdh5*, indicating that EUK-189 did not modulate NOTCH1 activity.

Discussion

The present study shows that PGC-1α plays an important role in the control of angiogenesis and in the stability of the mature vasculature. In the absence of PGC-1α, the vascular endothelium appears to be constitutively activated, probably due to elevated ROS levels that cause constitutive activation of the VEGF-A signaling pathway. These alterations are likely to be relevant in diabetic retinopathy where PGC-1α activity is generally found to be low.

The physiological consequences of PGC-1α deficiency in angiogenesis were analyzed in the retinas of PGC-1$\alpha^{-/-}$ mice. The retinal vasculature showed clear signs of instability, including a reduction in endothelial intercellular junctions and a significant loss of pericyte coverage. Furthermore, tip cells could be found in what should be quiescent vessels and displayed a lack of polarity. Reduced pericyte coverage is unlikely to be the result of defective recruitment but rather to their ulterior loss since pericytes were found in regions of active angiogenic activity. These alterations closely resemble those observed in diabetic retinopathy; however, VEGF-A protein levels were comparable in retinas from both groups of mice suggesting that differences in VEGF-A levels were not responsible for the observed phenotype.

Since elevated VEGF-A levels are generally regarded to be the main driver of the formation of anomalous blood vessels in diabetic retinopathy [20], we used the OIR protocol that recapitulates most if not all features of human diabetic retinopathy to question how PGC-1α-deficient mice respond to VEGF-A. OIR exacerbated the vascular instability observed under basal conditions in PGC-1$\alpha^{-/-}$ mice. The number of anomalous blood vessels was unaffected by the loss of PGC-1α, but these vessels were larger, fully collapsed and/or largely irregular in diameter. Analysis of the VEGF-A signaling pathway suggested that in wild-type animals OIR induces an activation of the pathway, while in PGC-1$\alpha^{-/-}$ animals the pathway is constitutively active and is non-responsive to elevated VEGF-A levels. Importantly, HIF-1α levels are more strongly induced in PGC-1$\alpha^{-/-}$-deficient mice and could account for the exacerbation of the phenotype.

PGC-1α-deficient ECs have elevated levels of ROS [7], and antioxidant treatment re-establishes the normal motility of PGC-1α-deficient ECs [9]. Given that the VEGF-A signaling pathway has been shown to be ROS sensitive [18, 21, 22], we hypothesized that elevated ROS could be responsible for the observed phenotype. Consistent with this hypothesis, antioxidant treatment partially restored vascular structure and VEGF-A signaling in PGC-1α-deficient mice.

It is generally acknowledged that pericyte coverage is essential for vessel stabilization, and there are several pathways involved in the intimate cross talk between the vascular endothelial cell and the pericyte. As a result, endothelial dysfunction generally results in pericyte loss and vice versa. Among the pathways involved, the TGF-β and the angiotensin system have been extensively characterized [23]. Importantly, the VEGFR2 has also been shown to be involved in this regulatory process [24]. In light of the previous evidence showing that loss of PGC-1α results in enhanced cell migration and of the present results suggesting that loss of PGC-1α alters the VEGFR2 signaling pathway, it is possible that this alteration may be responsible for the observed loss in pericyte coverage, although alternative scenarios are also possible.

Importantly, recent reports suggest a connection between the TGF-β pathway and PGC-1α [25].

That antioxidant treatment was not sufficient for a complete functional recovery in OIR-treated PGC-1α$^{-/-}$ retina raises several questions. It could be considered that since ROS are part of the normal signaling processes, complete detoxification of ROS cannot be expected to be fully beneficial [26]. Another reasonable possibility is that part of this phenotype cannot be attributed to ROS alone and might involve other PGC-1α target genes.

An attractive hypothesis is that PGC-1α might be necessary to recover the endothelial oxidative capacity following the "ischemic" period. In the OIR model, hyperoxia produces vasoconstriction that results in tissue hypoxia, activation of HIF-1α, and HIF-1α-dependent induction of VEGF-A [27]. HIF-1α activates glycolytic metabolism to prevent cell death during hypoxia [28]; however, excessive HIF-1α activity prevents the re-activation of oxidative metabolism and stabilization of the newly formed vasculature by an unknown mechanism. This inability to perfuse results in organ damage, e.g., cardiac hypertrophy [29]. Therefore, it is possible that the exacerbation of the vascular anomalies observed in OIR-treated animals and the partial effect of antioxidants can be attributed to the inability of ECs to reinitiate oxidative metabolism following HIF-1α activation, in the absence of PGC-1α.

In conclusion, our study supports the idea that PGC-1α plays a major role in the control of angiogenesis and is likely to be relevant in diabetic retinopathy. Furthermore, it suggests that constitutive activation of the VEGF-A signaling pathway can limit the therapeutic potential of VEGF-A-based therapies in the absence of a good redox balance. Future studies should be directed to investigate this re-wiring of normal ROS homeostasis.

Acknowledgments We thank Enrique Samper (NIMGenetics, Madrid, Spain) for providing EUK-189 and technical advice on its handling and use in experimental models. We thank Santiago Lamas and Maria Angeles Higueras (CBMSO, Madrid, Spain) for careful reading of the manuscript. We thank Kenneth McCreath for editorial support. This work was supported by grants from the Spanish ''Ministerio de Economía y Competitividad'' (Grant number SAF2009-07599 & SAF2012-37693 to M.M and CSD 2007-00020 to M.M.) and the ''Comunidad de Madrid'' (Grant Number S2010/BMD-2361 to M.M.).

Compliance with ethical standards

Conflict of interest The authors declare that they have no conflict of interest.

Human and animal rights This article does not contain any studies with human participants performed by any of the authors. All applicable international, national, and/or institutional guidelines for the care and use of animals were followed. All procedures performed in studies involving animals were in accordance with the ethical standards of the institution or practice at which the studies were conducted.

References

1. Theuma P, Fonseca VA (2003) Novel cardiovascular risk factors and macrovascular and microvascular complications of diabetes. Curr Drug Targets 4(6):477–486
2. Antonetti DA, Klein R, Gardner TW (2012) Diabetic retinopathy. N Engl J Med 366(13):1227–1239. doi:10.1056/NEJMra1005073
3. Rogge MM (2009) The role of impaired mitochondrial lipid oxidation in obesity. Biol Res Nurs 10(4):356–373. doi:10.1177/1099800408329408
4. Joseph AM, Joanisse DR, Baillot RG, Hood DA (2012) Mitochondrial dysregulation in the pathogenesis of diabetes: potential for mitochondrial biogenesis-mediated interventions. Exp Diabetes Res. doi:10.1155/2012/642038
5. Mootha VK, Lindgren CM, Eriksson KF, Subramanian A, Sihag S, Lehar J, Puigserver P, Carlsson E, Ridderstrale M, Laurila E, Houstis N, Daly MJ, Patterson N, Mesirov JP, Golub TR, Tamayo P, Spiegelman B, Lander ES, Hirschhorn JN, Altshuler D, Groop LC (2003) PGC-1α-responsive genes involved in oxidative phosphorylation are coordinately downregulated in human diabetes. Nat Genet 34(3):267–273. doi:10.1038/ng1180
6. Holloway GP, Perry CG, Thrush AB, Heigenhauser GJ, Dyck DJ, Bonen A, Spriet LL (2008) PGC-1α's relationship with skeletal muscle palmitate oxidation is not present with obesity despite maintained PGC-1α and PGC-1β protein. Am J Physiol Endocrinol Metab 294(6):E1060–1069. doi:10.1152/ajpendo.00726.2007
7. Olmos Y, Valle I, Borniquel S, Tierrez A, Soria E, Lamas S, Monsalve M (2009) Mutual dependence of Foxo3a and PGC-1α in the induction of oxidative stress genes. J Biol Chem 284(21):14476–14484. doi:10.1074/jbc.M807397200
8. Valle I, Alvarez-Barrientos A, Arza E, Lamas S, Monsalve M (2005) PGC-1α regulates the mitochondrial antioxidant defense system in vascular endothelial cells. Cardiovasc Res 66(3):562–573
9. Borniquel S, Garcia-Quintans N, Valle I, Olmos Y, Wild B, Martinez-Granero F, Soria E, Lamas S, Monsalve M (2010) Inactivation of Foxo3a and subsequent downregulation of PGC-1α mediate nitric oxide-induced endothelial cell migration. Mol Cell Biol 30(16):4035–4044. doi:10.1128/MCB.00175-10
10. West XZ, Malinin NL, Merkulova AA, Tischenko M, Kerr BA, Borden EC, Podrez EA, Salomon RG, Byzova TV (2010) Oxidative stress induces angiogenesis by activating TLR2 with novel endogenous ligands. Nature 467(7318):972–976. doi:10.1038/nature09421
11. Smith LE, Wesolowski E, McLellan A, Kostyk SK, D'Amato R, Sullivan R, D'Amore PA (1994) Oxygen-induced retinopathy in the mouse. Investig Ophthalmol Vis Sci 35(1):101–111
12. Hinerfeld D, Traini MD, Weinberger RP, Cochran B, Doctrow SR, Harry J, Melov S (2004) Endogenous mitochondrial oxidative stress: neurodegeneration, proteomic analysis, specific respiratory chain defects, and efficacious antioxidant therapy in superoxide dismutase 2 null mice. J Neurochem 88(3):657–667
13. Olmos Y, Sanchez-Gomez FJ, Wild B, Garcia-Quintans N, Cabezudo S, Lamas S, Monsalve M (2013) SirT1 regulation of antioxidant genes is dependent on the formation of a FoxO3a/PGC-1α complex. Antioxid Redox Signal 19:1507–1521. doi:10.1089/ars.2012.4713
14. Arany Z, Foo SY, Ma Y, Ruas JL, Bommi-Reddy A, Girnun G, Cooper M, Laznik D, Chinsomboon J, Rangwala SM, Baek KH,

Rosenzweig A, Spiegelman BM (2008) HIF-independent regulation of VEGF and angiogenesis by the transcriptional coactivator PGC-1α. Nature 451(7181):1008–1012

15. Saint-Geniez M, Jiang A, Abend S, Liu L, Sweigard H, Connor KM, Arany Z (2013) PGC-1α regulates normal and pathological angiogenesis in the retina. Am J Pathol 182(1):255–265. doi:10.1016/j.ajpath.2012.09.003
16. Sawada N, Jiang A, Takizawa F, Safdar A, Manika A, Tesmenitsky Y, Kang KT, Bischoff J, Kalwa H, Sartoretto JL, Kamei Y, Benjamin LE, Watada H, Ogawa Y, Higashikuni Y, Kessinger CW, Jaffer FA, Michel T, Sata M, Croce K, Tanaka R, Arany Z (2014) Endothelial PGC-1α mediates vascular dysfunction in diabetes. Cell Metab 19(2):246–258. doi:10.1016/j.cmet.2013.12.014
17. Lange C, Ehlken C, Stahl A, Martin G, Hansen L, Agostini HT (2009) Kinetics of retinal vaso-obliteration and neovascularisation in the oxygen-induced retinopathy (OIR) mouse model. Graefes Arch Clin Exp Ophthalmol 247(9):1205–1211. doi:10.1007/s00417-009-1116-4
18. Kang DH, Lee DJ, Lee KW, Park YS, Lee JY, Lee SH, Koh YJ, Koh GY, Choi C, Yu DY, Kim J, Kang SW (2011) Peroxiredoxin II is an essential antioxidant enzyme that prevents the oxidative inactivation of VEGF receptor-2 in vascular endothelial cells. Mol Cell 44(4):545–558. doi:10.1016/j.molcel.2011.08.040
19. Ushio-Fukai M (2006) Redox signaling in angiogenesis: role of NADPH oxidase. Cardiovasc Res 71(2):226–235
20. Gupta N, Mansoor S, Sharma A, Sapkal A, Sheth J, Falatoonzadeh P, Kuppermann B, Kenney M (2013) Diabetic retinopathy and VEGF. Open Ophthalmol J 7:4–10. doi:10.2174/1874364101307010004
21. Lee M, Choy WC, Abid MR (2011) Direct sensing of endothelial oxidants by vascular endothelial growth factor receptor-2 and c-Src. PLoS One 6(12):e28454. doi:10.1371/journal.pone.0028454
22. Oshikawa J, Urao N, Kim HW, Kaplan N, Razvi M, McKinney R, Poole LB, Fukai T, Ushio-Fukai M (2010) Extracellular SOD-derived H_2O_2 promotes VEGF signaling in caveolae/lipid rafts and post-ischemic angiogenesis in mice. PLoS One 5(4):e10189. doi:10.1371/journal.pone.0010189
23. Armulik A, Abramsson A, Betsholtz C (2005) Endothelial/pericyte interactions. Circ Res 97(6):512–523. doi:10.1161/01.RES.0000182903.16652.d7
24. Lin SL, Chang FC, Schrimpf C, Chen YT, Wu CF, Wu VC, Chiang WC, Kuhnert F, Kuo CJ, Chen YM, Wu KD, Tsai TJ, Duffield JS (2011) Targeting endothelium-pericyte cross talk by inhibiting VEGF receptor signaling attenuates kidney microvascular rarefaction and fibrosis. Am J Pathol 178(2):911–923. doi:10.1016/j.ajpath.2010.10.012
25. Tiano JP, Springer DA, Rane SG (2015) SMAD3 negatively regulates serum irisin and skeletal muscle FNDC5 and peroxisome proliferator-activated receptor gamma coactivator 1-α (PGC-1α) during exercise. J Biol Chem 290(18):11431. doi:10.1074/jbc.A114.617399
26. Oshikawa J, Kim SJ, Furuta E, Caliceti C, Chen GF, McKinney RD, Kuhr F, Levitan I, Fukai T, Ushio-Fukai M (2012) Novel role of p66Shc in ROS-dependent VEGF signaling and angiogenesis in endothelial cells. Am J Physiol Heart Circ Physiol 302(3):H724–732. doi:10.1152/ajpheart.00739.2011
27. Weidemann A, Johnson RS (2008) Biology of HIF-1α. Cell Death Differ 15(4):621–627
28. Rajabi M, Kassiotis C, Razeghi P, Taegtmeyer H (2007) Return to the fetal gene program protects the stressed heart: a strong hypothesis. Heart Fail Rev 12(3–4):331–343. doi:10.1007/s10741-007-9034-1
29. Shiojima I, Walsh K (2006) Regulation of cardiac growth and coronary angiogenesis by the Akt/PKB signaling pathway. Genes Dev 20(24):3347–3365